

Bulletin of Pioneering Researches of Medical and Clinical Science

Available online: https://bprmcs.com 2022 | Volume 1 | Issue 1 | Page: 69-84

Positive Impact of Weight Loss from Bariatric Surgery on the Proteomic Profile of Abdominal Subcutaneous Adipose Tissue

Carina Bona^{1,2}, Roberto Lozano^{1,2,3*}, Yanela Aravena-Rivas^{2,3,4}

¹Centro de Investigación Biomédica en Red de Diabetes y Enfermedades Metabólicas Asociadas (CIBERDEM), Instituto de Salud Carlos III (ISCIII), 28029 Madrid, Spain.

² Translational Research in Diabetes, Lipids and Obesity, Institut d'Investigacions Biomèdiques August Pi I Sunyer (IDIBAPS), 08036 Barcelona, Spain.

³ Obesity Unit, Endocrinology and Nutrition Department, Hospital Clínic de Barcelona, 08036 Barcelona, Spain.
⁴Centro de Investigación Biomédica en Red Fisiopatologia de la Obesidad y Nutrición (CIBEROBN), Instituto de Salud Carlos III (ISCIII), 28029 Madrid, Spain.

Abstract

Bariatric surgery (BS) remains the most effective strategy for treating obesity, offering notable improvements in cardiometabolic health and promoting remission of type 2 diabetes. The majority of post-surgical fat loss occurs in the subcutaneous adipose tissue (SAT), yet the functional changes within this depot and its precise role in the benefits of BS are still debated. To explore alterations in protein expression and associated molecular pathways in abdominal SAT (aSAT) following weight normalization induced by BS, we applied a proteomic strategy using sequential window acquisition of all theoretical mass spectra (SWATH-MS), complemented with Western blot, electron microscopy, and RT-qPCR analyses. Our study revealed that BS upregulated proteins involved in energy metabolism, the citric acid cycle, respiratory electron transport, triglyceride breakdown, ATP generation, pyruvate metabolism, glycolysis/gluconeogenesis, and thermogenic processes. Conversely, proteins associated with immune-related pathways were downregulated. We also observed that obesity led to reduced mitochondrial density and coverage in SAT, a defect that BS effectively reversed. These findings uncover specific proteins, genes, and molecular mechanisms that contribute to improved adipose tissue function after BS, including diminished inflammation, enhanced glucose uptake, increased insulin sensitivity, elevated de novo lipogenesis, improved mitochondrial performance, and smaller adipocyte size.

Keywords: Bariatric surgery,
Mitochondria, Proteome,
Abdominal adipose tissue,
Lipogenesis, Metabolism, Immune
system

Corresponding author: Roberto

Lozano

E-mail: Robertolozano@outlook.com

How to Cite This Article: Bona C, Lozano R, Yanela Aravena-Rivas Y. Positive Impact of Weight Loss from Bariatric Surgery on the Proteomic Profile of Abdominal Subcutaneous Adipose Tissue. Bull Pioneer Res Med Clin Sci. 2022;1(1):69-84. https://doi.org/10.51847/LEF23BdF8y

Introduction

Excessive expansion of adipose tissue (AT) underlies obesity, a chronic condition [1] that is difficult to manage and represents one of the fastest growing public health challenges globally, affecting both developed and

developing nations [2,3]. Obesity is multifactorial and strongly associated with increased mortality and a range of comorbidities, including type 2 diabetes (T2D), metabolic syndrome (MetS), hypertension, dyslipidemia, certain cancers, cellular senescence [4], sleep apnea, and osteoarthritis [5, 6]. It has also been linked to cognitive decline, including dementia and mild cognitive

impairment [7]. Importantly, obesity does not always translate into metabolic disease. According to the "expandability hypothesis," metabolic health is influenced less by total AT and more by fat deposition in non-adipose tissues, which can disrupt metabolic homeostasis [8].

Human AT can be broadly categorized into subcutaneous (SAT) and visceral (VAT) compartments. SAT constitutes over 80% of total body fat and is further subdivided into central (abdominal) and peripheral (gluteal-femoral) depots, each exhibiting distinct functional characteristics [9]. Evidence indicates that fat distribution is closely linked to insulin resistance, with VAT serving as the strongest predictor of cardiometabolic risk [10,11]. While SAT has traditionally been considered metabolically neutral—surgical removal of large SAT volumes (>10 kg) by liposuction does not consistently improve insulin sensitivity or other metabolic parameters [12]—some studies suggest a protective role for SAT, potentially via higher adiponectin levels [13]. Nevertheless, recent research highlights that abdominal SAT (aSAT), in contrast to gluteal-femoral fat, may also contribute to insulin resistance, with central fat negatively correlating with adiponectin levels regardless of its visceral or subcutaneous location [14]. Vegiopoulos et al. (2017) demonstrated that insulin-resistant obese further individuals exhibit reduced storage capacity, larger adipocytes, heightened inflammation, immune cell infiltration, an adverse adipokine profile, and increased fibrosis compared with insulin-sensitive counterparts [15]. Despite this, the precise contribution of aSAT to metabolic dysfunction remains a subject of debate.

Bariatric surgery (BS) is widely regarded as the most effective intervention for obesity, improving cardiometabolic outcomes and often inducing remission of T2D. Remarkably, improvements in glucose metabolism frequently precede significant weight loss, suggesting mechanisms beyond mere reduction in fat mass, though these mechanisms are not fully elucidated [16]. Studies have also linked decreases in waist circumference post-BS to a higher likelihood of T2D remission [17-19]. Considering that SAT accounts for the majority of fat loss following BS [20], it is plausible that changes in SAT mass and function contribute substantially to the metabolic benefits of surgery. To comprehensively investigate molecular changes in aSAT following BS-induced weight normalization, we employed a proteomic approach to map altered pathways. Paired biopsies underwent qualitative and quantitative LC-MS/MS analysis for protein identification and quantification. Selected proteomic findings were validated by Western blotting of lipogenic and insulin signaling proteins, while mRNA levels of genes related to metabolism and inflammation were measured. Additionally, mitochondrial parameters

(density, coverage, area) and adipocyte size distribution were assessed.

Materials and Methods

Patients and sample collection

This study was approved by the Research Ethics Committee of Galicia, Spain (reference 2014/135), and all participants provided written informed consent. Abdominal SAT samples were collected from three groups: morbidly obese patients undergoing bariatric surgery (Roux-en-Y gastric bypass or sleeve gastrectomy), the same patients after reaching a BMI < 30 kg/m² during abdominoplasty, and healthy non-obese controls undergoing hernia repair. Samples were collected intraoperatively without altering surgical protocols. Each biopsy was divided into three portions: one snap-frozen in dry ice and stored at –80 °C for molecular analyses, one paraffin-embedded, and one processed later for electron microscopy.

Protein identification by LC-MS/MS

Total protein extracts were prepared in lysis buffer (pH 7.5) containing 50 mM Trizma-HCl, 1 mM EGTA, 1 mM EDTA, 50 mM NaF, 5 mM sodium pyrophosphate, 1 mM sodium orthovanadate, 1 percent Triton X-100, a protease inhibitor cocktail (complete Mini EDTA-free; Roche Diagnostics), 0.25 M sucrose, and 0.1 percent βmercaptoethanol. Lysates were centrifuged at 12,000×g for 30 min at 4 °C. For LC-MS/MS analysis, 100 μg of protein from four patients pre- and post-BS was denatured in SDS-loading buffer (62.5 mM Trizma-HCl pH 6.8, 5 percent SDS, 10 percent glycerol, 5 percent βmercaptoethanol, 0.0025 percent bromophenol blue) for 5 min and loaded onto a 10% SDS-PAGE gel, stopping when the dye front entered 3 mm into the resolving gel [21, 22]. Proteins were visualized with Sypro-Ruby (Lonza, Switzerland), excised, and digested in-gel with trypsin as previously described [23]. Peptides were extracted through three consecutive 20-min incubations in 40 µL of percent acetonitrile/0.5% НСООН, concentrated in a SpeedVac, and stored at -20 °C for further analysis.

Mass spectrometry using shotgun DDA

For peptide separation, $4 \,\mu\text{L}$ ($4 \,\mu\text{g}$) of digested samples were injected into a micro-liquid chromatography system (Eksigent nanoLC 400, AB SCIEX, Madrid, Spain) interfaced with a high-speed TripleTOF 6600 mass spectrometer (AB SCIEX) equipped with a microflow source. Analytical separation was achieved using a Chrom XP C18 column ($150 \, \text{mm} \times 0.3 \, \text{mm}$, $3 \, \mu\text{m}$ particle size, $120 \, \text{Å}$ pore size; Eksigent), while a YMC-TRIART C18 trap column ($3 \, \mu\text{m}$, $120 \, \text{Å}$; YMC Europe GmbH) functioned inline to concentrate peptides before entering

the analytical column. The loading pump delivered 0.1% formic acid in water at $10\,\mu\text{L/min}$, whereas the gradient pump ran at $5\,\mu\text{L/min}$ using mobile phase A (0.1% formic acid in water) and mobile phase B (0.1% formic acid in acetonitrile). Peptide elution followed a 90-minute gradient, ramping from 2% to 90% B.

MS data acquisition employed a data-dependent strategy on the TripleTOF 6600 system (ASSY. N° 5060890), with the following source parameters: ion spray voltage 5500 V, curtain gas 25, collision energy 10, and gas 1 (GS1) 25. The software Analyst TF 1.7.1 controlled operation. Selection of precursor ions required m/z 350–1400, charge states 2–5, mass tolerance of 250 ppm, and minimum intensity of 200 counts. Previously fragmented ions were excluded for 15 s, and instrument calibration was performed every four hours using PepCalMix peptides.

Data processing

MS/MS files were processed using ProteinPilotTM 5.0.1 (AB SCIEX), employing the ParagonTM algorithm for sequence matching and ProgroupTM for protein grouping. Searches were conducted against a human-specific Uniprot database with iodoacetamide as the Cys alkylation and methionine oxidation as fixed modifications. Only identifications with a global false discovery rate $\leq 1\%$ were retained, based on a non-linear fitting approach [24].

Label-Free quantitation using SWATH-MS

Spectral library construction

To build the SWATH spectral library, pooled peptide mixtures representing all study groups were analyzed using the same shotgun DDA micro-LC-MS/MS setup. Each 4 μ L pooled sample underwent separation using a 40-minute gradient (5%–95% B over 30 min, followed by 5 min at 90% B and 5 min re-equilibration at 5% B). MS acquisition consisted of a 250 ms survey scan (400–1250 m/z) followed by 25 ms MS/MS scans of the top 65 precursor ions (100–1500 m/z), with a total cycle of 2.8 s. Fragmented ions were dynamically excluded for 15 s, and singly charged species were ignored.

Peptide and protein identification was performed in ProteinPilot™ 5.0.1 using the same Uniprot human database and modification settings. A 1% FDR cutoff was applied at both the peptide and protein levels. The high-confidence spectra (≥99% confidence) were then used to generate the SWATH library in PeakView 2.2 with the MS/MSALL SWATH Acquisition MicroApp 2.0, enabling subsequent label-free quantification.

Relative quantification using SWATH-MS

Eight abdominal SAT samples were analyzed, comprising four from morbidly obese patients and four from the same

individuals after bariatric surgery once their BMI was below 30. Each sample (4 µL) was processed using the LC–MS/MS setup and gradient previously described for spectral library generation, but acquisition was performed with the SWATH-MS data-independent method. This approach consisted of sequentially cycling through 65 overlapping precursor isolation windows (with 1 m/z overlap) spanning the 400–1250 m/z range. Each cycle included a preceding TOF MS scan (400–1250 m/z, 50 ms) followed by the 65 MS/MS scans (400–1500 m/z, high-sensitivity mode, 50 ms per scan), resulting in a total cycle time of 6.3 s. Window widths were optimized for each set using ion density data from prior DDA runs and the SWATH variable window calculator provided by Sciex.

Data analysis

Extraction of fragment ion chromatograms from the SWATH runs was performed in PeakView 2.2 using the SWATH Acquisition MicroApp 2.0, referencing the spectral library generated from the DDA analysis. For each protein, up to ten peptides and seven fragments per peptide were selected based on signal intensity, excluding modified peptides. Ion chromatograms were extracted with a 5-minute retention window and 30 ppm width. After alignment of retention times, integrated peak areas were exported to MarkerView 1.3.1 (AB SCIEX) for relative quantification. MarkerView performed data alignment to correct minor variations in mass and retention time, ensuring accurate comparisons across samples. To account for possible differences in sample preparation, peak areas were globally normalized to the total sum of all detected transitions for each replicate. Unsupervised multivariate analysis using principal component analysis (PCA) with Pareto scaling was conducted to compare the samples (data not shown). The mean peak area per protein across replicates was calculated and subjected to Student's t-test in MarkerView to assess differences between groups, with statistical significance reported as p-values. Proteins displaying a p-value <0.5 and at least a 1.5-fold change were considered differentially expressed.

Gene ontology, functional networks, and pathway mapping

To explore functional implications of weight-dependent protein changes, qualitative protein datasets—those detected only during obesity or post-weight normalization—were analyzed for enrichment in gene ontology (GO) categories, protein classes, and biological pathways using the PANTHER tool (version 14.1, www.pantherdb.org) [25]. For quantitative datasets of proteins up- or down-regulated after bariatric surgery, GO enrichment was performed using FunRich (version 3.1.3, http://www.funrich.org) [26]. Reactome pathway analysis

for differentially expressed proteins after weight loss was conducted with STRING (version 11, https://string-db.org) [27]. Only proteins with statistically significant changes were included. Heatmaps representing expression patterns were generated using matrix2png (version 1.2.2, http://www.chibi.ubc.ca/matrix2png/).

Western blot analysis

Protein expression levels of fatty acid synthase (FAS), AKT, phosphorylated AKT (pAKT), acetyl-CoA carboxylase (ACC), phosphorylated ACC (pACC), AMPKα1, phosphorylated AMPKα (pAMPKα), and glyceraldehyde 3-phosphate dehydrogenase (GAPDH) were evaluated in aSAT samples using Western blot. Total protein extracts were prepared as described previously. For each sample, 15 µg of protein lysate was denatured in SDS-loading buffer for 5 min at 100 °C and separated by SDS-PAGE (7 percent or 10 percent gels), followed by transfer onto polyvinylidene fluoride membranes (Millipore). Membranes were blocked for 1 h at room temperature in 5% BSA prepared in 1× Tween-Trisbuffered saline (TTBS; 25 mM Tris-HCl, 150 mM NaCl, 0.05% Tween-20, pH 7.5) and washed three times with TTBS. Primary antibodies were incubated overnight at 4°C: ACC and pACC-Ser79 (Millipore); AMPKα1, pAMPKα-Thr172, AKT, pAKT-Ser473 (Cell Signaling); FAS (Santa Cruz Biotechnology); and GAPDH (Thermo Fisher Scientific). Following washing, membranes were incubated with horseradish peroxidase-conjugated secondary antibodies (Dako) for 1 h at room temperature. **Proteins** were detected using enhanced chemiluminescence (Pierce ECL, ThermoFisher) and imaged with an Amersham Imager 600 (GE Healthcare Life Sciences). Band intensities were quantified by densitometry with ImageJ software (v1.52a, NIH, USA) [28], and all protein levels were normalized to GAPDH.

Hexokinase (HK) activity assay

aSAT samples were homogenized in a 1:4 ratio with ice-cold buffer containing 20 mM Tris-HCl (pH 7.4), 250 mM sucrose, 1 mM EDTA, 1 mM dithiothreitol, 100 mM NaF, and protease inhibitor cocktail (Roche, Sweden). HK activity was determined by monitoring NADH formation at 340 nm using a microplate reader (Tecan, Sunrise). Reactions were initiated by adding 50 μL of homogenate and 20 μL of substrate (omitted in controls) to a final volume of 0.25 mL, and incubated at 37 °C for 5 min. Activity was assessed according to previously described methods with minor modifications [29] and normalized to total protein, which was measured using the Bradford assay (Bio-Rad) with bovine serum albumin as the standard.

Quantitative real-time PCR (RT-qPCR)

Total RNA was extracted from adipose tissue using TRIzol reagent (Invitrogen). RNA integrity was verified by agarose gel electrophoresis, and concentrations were measured using a NanoDrop ND-1000 spectrophotometer (Thermo Scientific). For cDNA synthesis, 0.8 µg of RNA per sample was reverse-transcribed in a 20 µL reaction using SuperScript IV reverse transcriptase and random hexamers (Invitrogen). Quantitative PCR was performed with SYBR Green qPCR Master Mix (Roche) on a Roche LightCycler 480 system. The primer sets used were:

- FBXL10: F 5'-TACGACGAGAACGAGGACTT, R 5'-AGGCATCTTAATTCCCAGTCCA
- IPO8: F 5'-ACAATGTGTCTCCGTGCCAT, R 5'-AGCTTGCACTGCTCTGTGAT
- ADH1B: F 5'-AAGGGGGCTGTTTATGGTGG, R 5'-ACGTCAGGACGGTACGGATA
- FAS: F 5'-CTGCACTTCCATAGCCCCAA, R 5'-AAGGAGTTGATGCCCACGTT
- SLC2A4/GLUT4: F 5'-CGTCGGGCTTCCAACAGATA, R 5'-CACCTTCTGAGGGGCATTGA
- S100A8: F 5'-TGTTGACCGAGCTGGAGAAA, R 5'-CCCTGTAGACGGCATGGAAAT

Relative expression levels were calculated using standard curves generated from serial dilutions of a reference cDNA sample. Gene expression was normalized to the geometric mean of the two reference genes, IPO8 and FBXL10. PCR cycling conditions included an initial denaturation at 95 °C for 10 min, followed by 40 cycles of 95 °C for 15 s, 60 °C for 55 s, 72 °C for 5 s, and a final extension at 72 °C for 10 min.

Electronic microscopy and mitochondrial quantification

Adipose tissue biopsies were immersed in a fixative solution containing 0.5 percent glutaraldehyde, 4 percent paraformaldehyde, and 15 percent picric acid in 0.1 M phosphate buffer (pH 7.4) and maintained at 4 °C for 48 hours. Samples were then stored at 4 °C in phosphate buffer with 0.1 percent sodium azide until further processing. After washing three times in phosphate buffer, 50 μm sections were prepared using a vibratome. The sections underwent osmium tetroxide post-fixation for 15 minutes and sequential dehydration in increasing ethanol concentrations. To enhance ultrastructural contrast, 1 percent uranyl acetate was incorporated into the 70% ethanol step. Subsequently, tissues were embedded flat in Durcupan resin. Ultrathin sections were produced with a Leica ultramicrotome, mounted on Formvar-coated single-slot grids, and examined using a Tecnai 12 Biotwin electron microscope equipped with an AMT XR-16 camera. Only clearly defined cells were included in the analysis. Mitochondrial parameters, including coverage, density, and aspect ratio, were measured using ImageJ software. Density was defined as the number of mitochondria per cytosolic area, while coverage was calculated as the proportion of cytosol occupied by mitochondria.

Assessment of adipocyte size

Tissue samples were fixed in 4% paraformaldehyde for 24 hours, dehydrated, and embedded in paraffin. Sections of 5 µm thickness were cut, deparaffinized, and rehydrated. Hematoxylin and eosin staining (Mayer's hematoxylin and 1% eosin Y) was applied according to established protocols [30]. After dehydration and clearing in xylene, slides were mounted with a resinous medium. Adipocyte dimensions were measured from microscope images acquired with an Olympus BX61, using the CellSens Dimension software to calculate cell size.

Statistical procedures

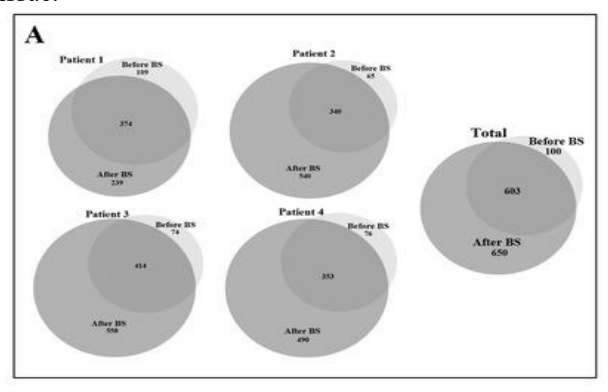
Proteomic data were processed as described previously. All other datasets were analyzed with SigmaStat 3.1 (Systat Software, Inc., Germany) and reported as mean \pm SEM. For datasets following a normal distribution, oneway ANOVA with Tukey's post hoc test was applied. Non-parametric datasets were assessed with the Kruskal–Wallis test followed by Dunn's post hoc test. Statistical significance was defined as p < 0.05. Distinct letters above graphical bars indicate statistically significant differences between groups.

Results

Qualitative proteomic profiling of aSAT pre- and post-weight reduction

To examine proteomic alterations associated with weight loss, paired aSAT samples from the same individuals were analyzed before and after bariatric surgery. Relevant anthropometric and biochemical characteristics of these patients are provided in **Table 1**. The qualitative proteomic analysis identified 1,353 proteins in total (**Figure 1A**). Of these, 100 proteins were exclusively present in the obese state, whereas 650 proteins were detected only after patients had reached normalized body weight. Six hundred and three proteins were common to both conditions. Notably, the number of proteins identified

increased following bariatric surgery (Figure 1A), indicating that obesity is associated with a reduction in protein diversity within abdominal subcutaneous adipose tissue.



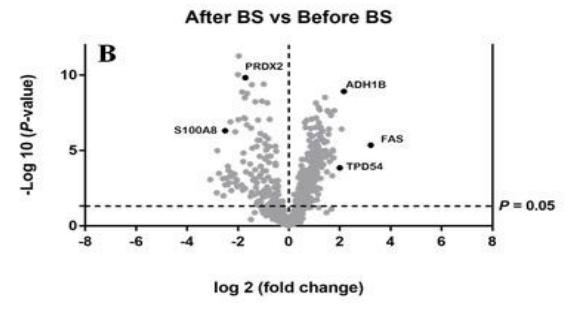


Figure 1. (A) Impact of obesity and bariatric surgery on protein profiles in the abdominal subcutaneous adipose tissue (aSAT). Venn diagrams depict the qualitative proteomic comparison of aSAT from four obese patients before bariatric surgery (pre-BS) and the same patients after weight normalization following bariatric surgery (post-BS). The diagrams show the number of proteins unique to each condition, as well as the overlap for each individual patient (Patients 1-4) and the total number of proteins detected. (B) Quantitative proteomic results are illustrated in a volcano plot, where proteins are plotted according to statistical significance (p-value, y-axis) and log2-transformed fold-change between post-BS and pre-BS aSAT samples (x-axis). Points located far from the center represent proteins with the largest differences between the two conditions. Proteins were considered significantly altered if foldchange ≥ 1.5 and p < 0.05.

Table 1. Anthropometric and biochemical parameters of patients used for mass spectrometric analysis											
Gender Type of Bariatric Surgery	Patient 1 Female Sleeve		Patient 2 Female Sleeve		Patient 3 Female Bypass		Patient 4 Male Sleeve				
	Before BS	After BS	Before BS	After BS	Before BS	After BS	Before BS	After BS			
Age (years)	45.3	+27 m	31.4	+33 m	58	+24 m	45.4	+22 m			
D2M	1	0	0	0	1	0	0	0			
Hypertension	1	0	0	0	1	0	0	0			
BMI (kg/m^2)	49.2	29.2	44.6	26.3	39.8	29.2	66.3	29.8			

FAT (%)	53	38.9	51.4	32.4	51.7	39.3	47.2	11.4
Medication	Amlodipine/Valsartan	Atorvastatin	0	0	Simvastatin Metformin Dapagliflozin	0	0	0
Glucose (mg/dL)	127	81	78	86	131	85	83	81
Cholesterol (mg/dL)	267	166	123	165	159	190	158	150
HDLc (mg/dL)	39	55	19	45	43	75	27	45
LDLc (mg/dL)	191	100	91	104	97	101	99	87
Triglycerides (mg/dL)	165	52	63	80	94	70	119	91
AST (UI/L)	27	13	21	14	61	76	28	22
ALT (UI/L)	36	9	18	10	51	99	70	20
GGT (UI/L)	68	19	17	14	40	37	96	35
Insulin (µUI/mL)	7.61	<2	3.3	3	11.4	3.1	8.1	<2
ApoA (mg/dL)	124	161	60.4	136	152	_	97.4	119
ApoB (mg/dL)	123	80.8	99.6	86.8	94.4	-	100	76.8
CRP (mg/dL)	2	0.32	0.88	0.02	1.5	_	1.33	0.01
HbA1c (%)	6.2	5	5.4	4.9	8	5.2	5.6	5.2
HOMA-IR	2.21	0.4	0.63	0.64	3.69	0.65	1.7	0.4

Abbreviations: BMI: body mass index; HDLc: high-density lipoprotein cholesterol; LDLc: low-density lipoprotein cholesterol; AST: aspartate aminotransferase; ALT: alanine aminotransferase; GGT: γ-glutamyltransferase; ApoA: Apolipoprotein A; ApoB: Apolipoprotein B; HbA1c: glycated hemoglobin; HOMA: homeostasis model assessment index; CRP: C-reactive protein; BS: bariatric surgery. (–) indicates data not available in the medical records.

The PANTHER classification system [25] was applied to proteins detected exclusively in either the obese state or after bariatric surgery-induced weight loss. Comparing the 100 proteins identified only during obesity with the 650 proteins unique to the post-weight loss condition revealed notable molecular effects associated with obesity and subsequent surgical weight reduction. Enriched gene ontology (GO) categories for cellular component, molecular function, and biological process summarized in Table S1, along with detailed analyses of protein classes and biological pathways. Following weight loss, the proportion of proteins linked to the extracellular region and cell junctions decreased, whereas proteins localized to organelles increased. Proteins associated with immune system processes and responses to external stimuli were reduced after weight normalization. Notably, a substantial number of proteins detected only postsurgery were implicated in diverse metabolic pathways (see Table S1 for details).

Quantitative analysis of differentially expressed proteins in aSAT before and after weight loss and bioinformatic enrichment

Using the criteria described above, a total of 651 proteins were quantitatively measured across all patients pre- and post-bariatric surgery (Table S2). To visualize the data, a volcano plot was constructed showing the log2 fold-change for each protein against its p-value (Figure 1B). Proteins were considered significantly altered if they had a p-value < 0.05 and a fold-change > 1.5. Following weight loss induced by bariatric surgery, 228 proteins were significantly up-regulated, while 136 proteins were significantly down-regulated. The expression levels of these differentially regulated proteins are presented in a heat map in Figure 2.

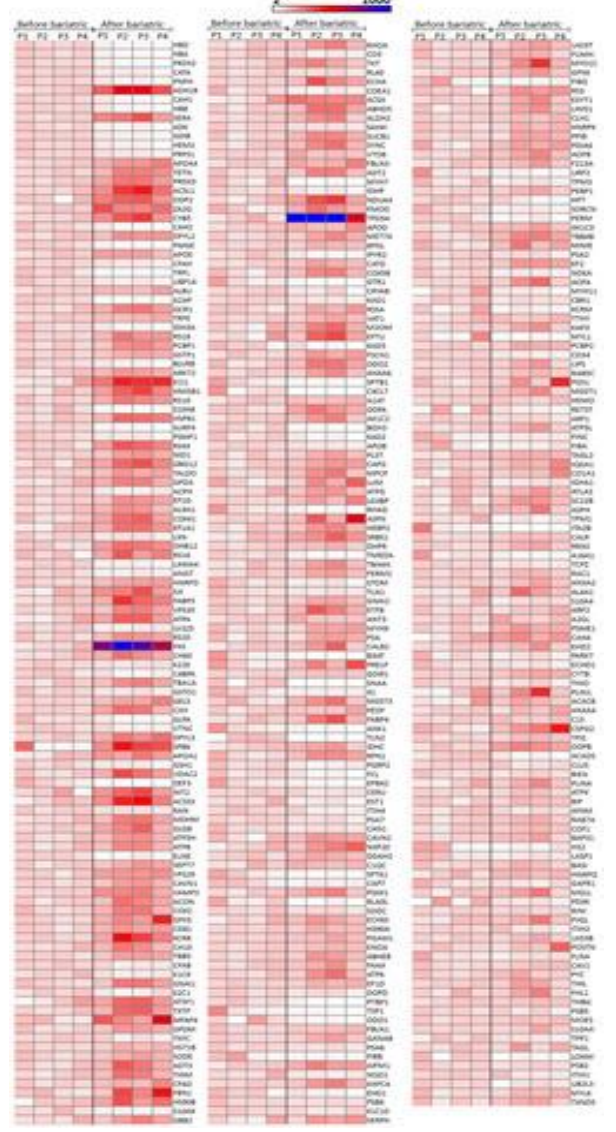


Figure 2. Heatmap showing proteins in abdominal subcutaneous adipose tissue (aSAT) that were significantly altered following bariatric surgery-induced weight loss, analyzed using the SWATH-MS technique. A total of 364 proteins were significantly

regulated, with 228 up-regulated and 136 down-regulated. Protein expression intensity is represented on a scale from white to blue in arbitrary units. To standardize visualization, expression values for each protein were normalized to the mean expression in the four patients before surgery, which was set as 100%. Proteins are arranged by p-value: the first column ranges from 5.25E–12 to 5.47E–05, the second from 5.97E–05 to 0.00283, and the third from 0.00284 to 0.04071. Statistical significance was defined as p < 0.05. Data were plotted using matrix2png version 1.2.2 (http://www.chibi.ubc.ca/matrix2png/). P1–P4 indicate Patients 1–4.

To explore functional categories of the proteins significantly modulated after weight normalization, the up- and down-regulated protein sets were analyzed using FunRich software, which applies a hypergeometric test for GO term enrichment [26].

In the GO enrichment analysis, both up- and downregulated proteins were largely associated with similar cellular compartments, including exosomes, cytoplasm, lysosomes, mitochondria, cytosol, extracellular regions, and centrosomes (Figure 3A). However, notable differences were observed: up-regulated proteins after weight loss showed stronger enrichment in mitochondria, including the mitochondrial matrix, inner membrane, and ATP synthase complex, whereas down-regulated proteins were more associated with extracellular components, nucleosomes, and the fibringen complex (Figure 3A). For molecular function, up-regulated proteins were predominantly linked to transporter activity, extracellular matrix interactions, structural constituents, and chaperone activity, while down-regulated proteins showed higher enrichment in structural molecule activity complement activity (Figure 3B). Regarding biological processes, the most enriched pathways involved metabolism and energy production, a pattern particularly evident among up-regulated proteins following weight loss (Figure 3C).

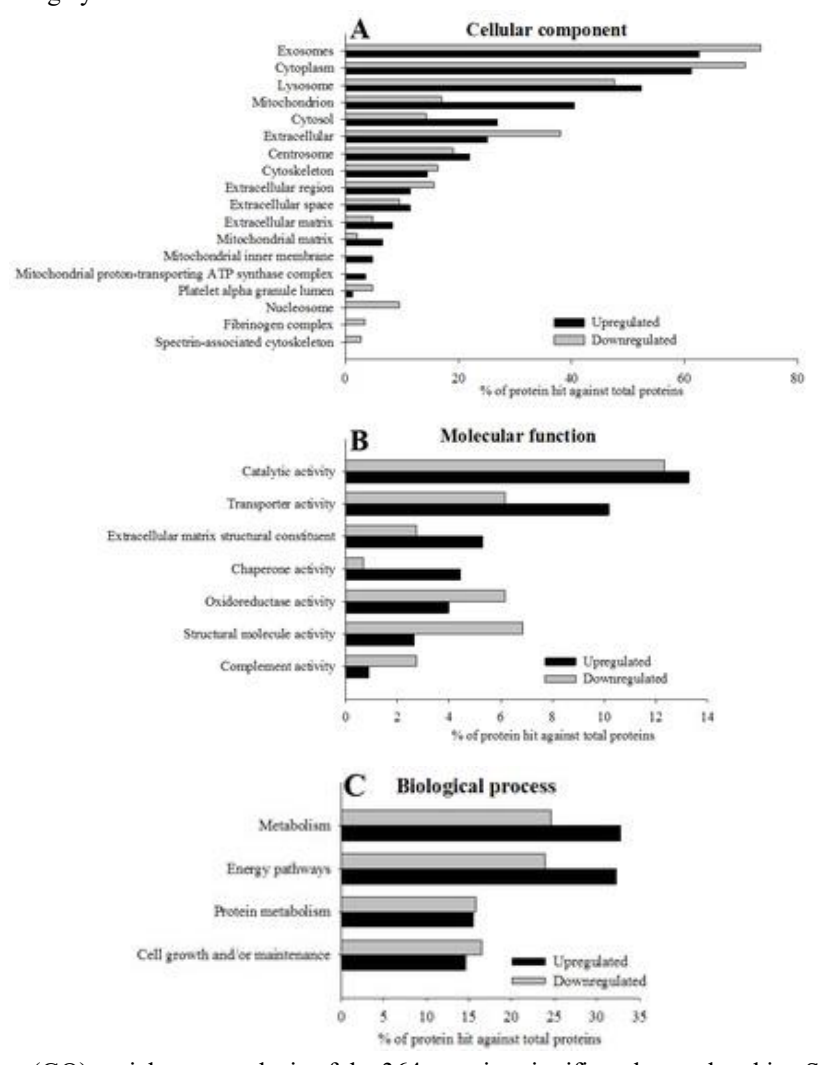


Figure 3. Gene ontology (GO) enrichment analysis of the 364 proteins significantly regulated in aSAT following bariatric surgery, performed using FunRich functional annotation. Histograms illustrate the most enriched categories for cellular component (A; $p < 10^{-5}$), biological process (B; p < 0.05), and molecular function (C; p < 0.05) for up- and down-regulated proteins quantified by SWATH-MS. Extended GO enrichment data are provided in Table S3

To gain deeper insights into the biological relevance of the changes induced by bariatric surgery and weight loss in aSAT, functional pathway enrichment analysis was conducted using the STRING reactome database (https://string-db.org/). Proteins up-regulated bariatric surgery, showing the most significant p-values, were mainly involved in metabolic processes, including the citric acid cycle, respiratory electron transport, triglyceride catabolism, ATP synthesis, metabolism, glycolysis/gluconeogenesis, and thermogenesis (Table S4). Conversely, down-regulated proteins with the lowest p-values were predominantly linked to immune system pathways (Table S4). These findings align with the observations from the qualitative proteomic analysis.

Collectively, these results indicate that bariatric surgery modulates key pathways in metabolism, energy production, and immune function in aSAT.

Validation of SWATH-MS results

It is well established in humans that impaired lipogenesis and increased lipolysis in adipose tissue can promote insulin resistance through the release of cytokines and lipid metabolites [31]. Following SWATH-MS quantification, we sought to validate the effects of obesity and bariatric surgery on key enzymes involved in de novo lipogenesis and insulin signaling. To this end, a control group of healthy individuals with normal BMI was included. Anthropometric and biochemical characteristics of these patients are summarized in Table S5, with enzymatic and protein data shown in **Figure 4A–C**.

We first examined hexokinase (HK) activity, as glucose phosphorylation limits downstream metabolic processes such as glycolysis and de novo lipogenesis. Obesity was associated with a marked reduction in HK activity, which was restored after weight normalization post-bariatric surgery. A similar trend was observed in protein levels of FAS, ACC (total expression phosphorylated), and AMPK (total and phosphorylated), the SWATH-MS results confirming for Interestingly, for both FAS and ACC, protein levels after weight loss not only returned to baseline but exceeded those of the control group, suggesting an enhanced capacity for de novo lipogenesis following bariatric surgery.

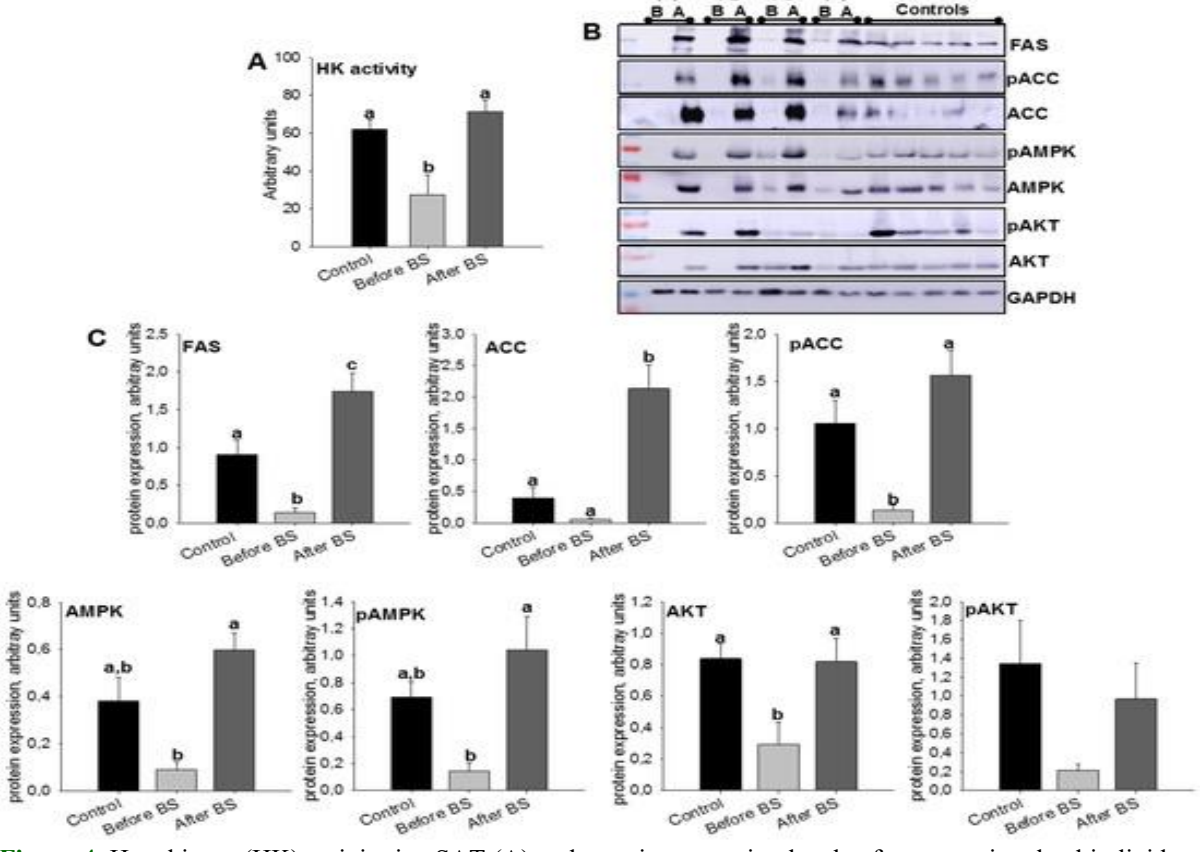
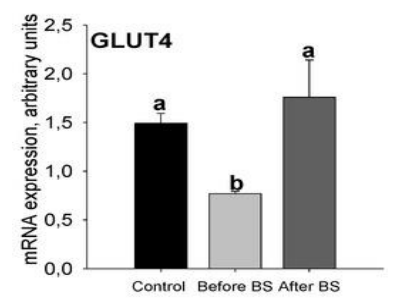


Figure 4. Hexokinase (HK) activity in aSAT (A) and protein expression levels of enzymes involved in lipid metabolism and insulin signaling (B, C) in control subjects, obese patients before bariatric surgery (BS), and the same patients after BS. Data represent means \pm SEM for six individuals per group (HK activity) or 4–5 per group (Western blot). Different letters above bars indicate statistically significant differences (p < 0.05). P.1–P.4 = Patient 1–Patient 4. "B" = before bariatric surgery, "A" = after bariatric surgery. Controls = healthy individuals with normal BMI

Insulin, a key endocrine hormone, plays a central role in regulating energy balance and lipid metabolism. In obesity, peripheral tissues often develop reduced insulin sensitivity [32]. Although the mechanisms underlying insulin resistance remain debated, AKT activation has been identified as a critical mediator [33]. Activated AKT promotes the translocation of GLUT4 to adipocyte membranes, facilitating glucose uptake [33]. As shown in **Figure 4B, C**, obesity reduced both total and phosphorylated AKT levels, which were restored following weight loss.

To reinforce the reliability of our proteomic and bioinformatic findings, we extended the analysis to examine mRNA expression of GLUT4 and key proteins involved in metabolism and inflammation that were highlighted in the SWATH-MS analysis: FAS, ADH1B, and S100A8. This approach allowed us to expand the sample size considerably for control subjects (n = 27) and obese patients before weight loss (n = 145). However, for post-bariatric surgery patients, sample collection was limited (n = 6) because many individuals, despite losing weight, did not meet the criteria for abdominoplasty (Table S6 presents anthropometric and biochemical data for these patients).

GLUT4 mRNA levels were reduced in the aSAT of obese individuals but returned to baseline after weight loss (Figure 5). These results parallel the changes observed in HK activity and AKT protein levels (Figure 4), indicating that glucose uptake is impaired during obesity, likely due to diminished insulin sensitivity, and is restored following body weight normalization. Similarly, FAS and ADH1B mRNA expression decreased markedly in obesity and rebounded after weight loss, in some cases exceeding control levels, although statistical significance was limited due to the small number of post-BS samples (Figure 5). Collectively, these findings suggest that obesity diminishes insulin sensitivity, glucose uptake, glycolysis, and de novo lipogenesis in aSAT, whereas bariatric surgery-induced weight loss effectively restores—and in some instances enhances—these metabolic functions compared with healthy controls.



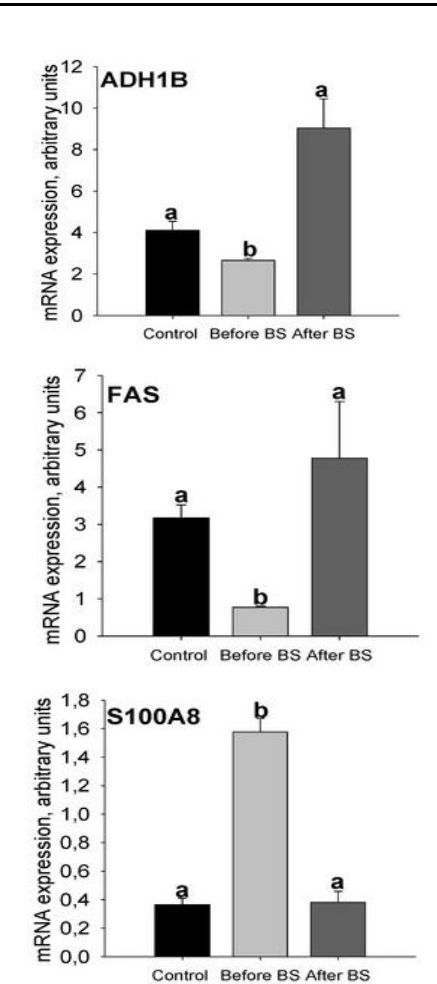


Figure 5. mRNA expression levels of GLUT4, FAS, S100A8, and ADH1B in aSAT from control subjects, obese patients before bariatric surgery (BS), and the same patients after BS and weight normalization. Data are presented as means \pm SEM. Different letters above bars indicate statistically significant differences (p < 0.05). Control = healthy subjects with normal BMI, n = 27; Before BS, n = 145; After BS, n = 6. BS = bariatric surgery

S100A8, a calcium- and zinc-binding protein, plays a key role in modulating inflammatory responses and immune system activity, including in cardiovascular disease [34]. Chronic, low-grade inflammation of adipose tissue is a major contributor to obesity pathophysiology [35], and elevated S100A8 in adipose tissue can enhance macrophage migration, promoting persistent local inflammation [36]. In line with this, the SWATH-MS analysis showed a marked reduction in S100A8 protein levels following bariatric surgery-induced weight loss. Correspondingly, S100A8 mRNA expression (Figure 5) was elevated in obesity but returned to levels comparable to controls after weight normalization, supporting the idea that BS-mediated weight loss mitigates adipose tissue inflammation.

Adipose tissue from insulin-resistant individuals also exhibits reduced expression of proteins involved in mitochondrial function, which limits the availability of mitochondria-derived energy required for lipogenesis [31]. Notably, many proteins upregulated after weight loss were associated with mitochondrial components (Figure 3A) and were implicated in pathways related to respiratory electron transport and ATP production (Table S2). To further investigate these observations, we analyzed mitochondrial morphology and metrics. Figure 6 illustrates mitochondrial aspect ratio (AR), density, and coverage. An AR of 1 represents a perfect circle, while

higher values reflect more elongated mitochondria. Obesity appeared to induce slightly elongated mitochondria, a trend that was reversed after weight loss, although not statistically significant (Figure 6A). Both mitochondrial density and coverage were reduced in obesity but were restored after bariatric surgery, in some cases exceeding levels observed in control subjects (Figure 6B,C).

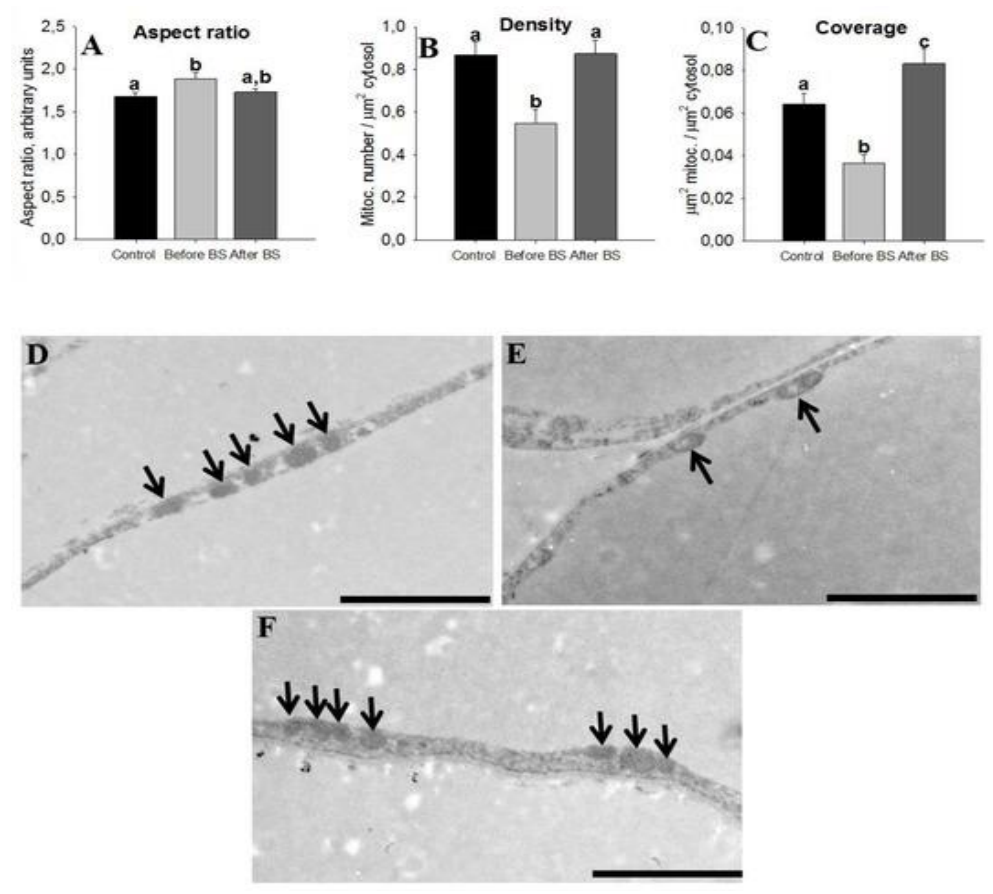


Figure 6. Mitochondrial Morphology. Mitochondrial characteristics were assessed in aSAT samples from healthy individuals (normal BMI, n = 5), obese patients before bariatric surgery (n = 4), and the same patients after surgery with normalized body weight (n = 5). Data are shown as mean \pm SEM, and statistically significant differences are indicated by different letters above bars (p < 0.05). The aspect ratio (AR), reflecting mitochondrial elongation, was calculated as the ratio between the major and minor axes (A). Mitochondrial density (B) and overall mitochondrial coverage (C) were determined by dividing the number of mitochondria or total mitochondrial area by the cytoplasmic area, respectively. Representative electron microscopy images of aSAT are displayed for controls (D), obese patients pre-surgery (E), and post-surgery (F). Scale bars = 2 μ m, arrows indicate mitochondria

Adipocyte size

Adipocyte diameters and their distribution were analyzed across the groups. Measurements included more than 5000 cells (1740 in controls, 1730 pre-surgery, and 1662 post-surgery). As shown in **Figure 7**, all groups demonstrated

a normal size distribution. Obese individuals exhibited larger adipocytes compared to controls and post-surgery patients. Following bariatric surgery, the average adipocyte size decreased slightly, even falling below the mean size observed in the healthy control group.

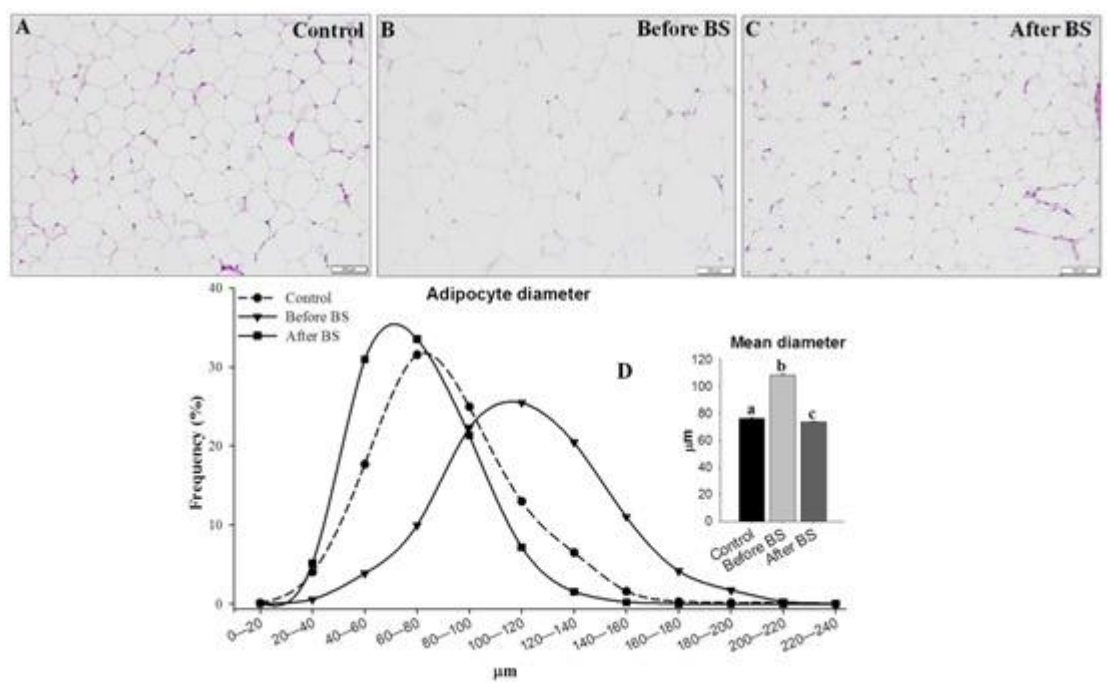


Figure 7. Distribution of Adipocyte Sizes. Representative H&E-stained sections of aSAT reveal differences in adipocyte size among lean control patients (A, n = 14), obese patients prior to bariatric surgery (B, n = 14), and the same patients following bariatric surgery with normalized body weight (C, n = 6). Panel D shows the average frequency distribution of adipocyte diameters, indicating that obese patients before surgery had a higher proportion of adipocytes larger than 80 μ m and fewer smaller than 80 μ m compared to either controls or post-surgery patients. Scale bars = 200 μ m. Data are presented as means \pm SEM, and statistically significant differences are indicated by different letters above the bars (p < 0.05). BS = bariatric surgery

Discussion

In total, more than 1300 proteins were identified, with 651 proteins quantitatively assessed. Following body weight normalization, the aSAT proteome exhibited markedly greater diversity. Specifically, 228 proteins were upregulated while 136 were down-regulated after weight loss. Notably, the up-regulated proteins were more highly associated with mitochondrial structures, including the mitochondrial matrix, inner membrane, and ATP synthase proton-transporting complex, whereas down-regulated proteins were enriched in components such as extracellular regions, nucleosomes, and the fibrinogen complex.

Pathway analysis of the altered proteins revealed that upregulated proteins were predominantly involved in metabolic processes, including the citric acid cycle, respiratory electron transport, triglyceride catabolism, ATP production, pyruvate metabolism, glycolysis/gluconeogenesis, and thermogenesis. In contrast, proteins that decreased after bariatric surgery were mainly associated with immune system-related pathways.

Validation using Western blot and RT-qPCR in an expanded cohort including lean controls confirmed that obesity reduced lipogenic enzyme expression, whereas

bariatric surgery restored and, in some cases, even enhanced these levels beyond those observed in controls. A similar trend was observed for GLUT4, FAS, and ADH1B mRNA expression, reflecting a "super-normal" state previously reported in women five years post-bariatric surgery, who showed higher insulin sensitivity compared to controls [37].

Subcutaneous adipose tissue (SAT) serves as the primary lipid storage site, yet its expansion capacity is limited. When expansion is insufficient, hypertrophic adipocytes develop, leading to reduced lipid storage efficiency, increased lipolysis, and ectopic fat deposition, all of which promote systemic insulin resistance. The limited storage capability of SAT is a key contributor to obesity-related metabolic complications [38, 39]. Enhancing the lipid storage capacity of adipose tissue may therefore prevent ectopic fat accumulation and maintain metabolic homeostasis.

Consistent with this, bariatric surgery-induced weight loss improved glucose uptake, as reflected by higher HK activity, and enhanced de novo lipogenesis, indicated by elevated ACC and FAS protein and mRNA levels. These changes occurred alongside improved insulin sensitivity, evidenced by reductions in HOMA-IR and fewer patients requiring T2D medication, as well as increased AKT levels. Furthermore, GLUT4 mRNA expression, the main insulin-responsive glucose transporter, was up-regulated

following bariatric surgery, which likely contributed to the observed increases in glucose uptake and lipogenesis in aSAT. Reduced GLUT4 and lipogenesis in adipocytes are known to impair synthesis of branched fatty acid esters of hydroxy fatty acids (FAHFAs), a lipid family secreted by adipose tissue that enhances insulin-stimulated glucose transport, promotes GLP-1 and insulin secretion, and exerts anti-inflammatory effects [40].

In humans, ADH1B expression is negatively associated with waist circumference, BMI, fasting plasma insulin [41], and adipocyte size [42], and it has also been linked to body weight regulation [43]. These observations have led to the suggestion that ADH1B may play a role in adipose tissue (AT) expandability [42]. In our study, both ADH1B protein and mRNA levels were reduced in obesity, but bariatric surgery (BS) not only restored these levels but in some cases surpassed those observed in the control group, reinforcing the inverse relationship between ADH1B and BMI, insulin resistance, and adipocyte size. While this does not conclusively confirm Voguel *et al.*'s hypothesis, it provides supporting evidence that aSAT expandability improves following BS.

Adipocytes adapt to excess energy through structural remodeling, which can manifest as hypertrophy or hyperplasia. Evidence suggests that hypertrophy is linked to relative insulin sensitivity or early stages of insulin resistance, whereas hyperplasia is associated with more pronounced insulin resistance and increased risk of type 2 diabetes (T2D) [44–47]. Individuals with a predominance of small adipocytes tend to exhibit impaired fat storage and adipogenesis, which increases their susceptibility to insulin resistance and T2D [48-50]. Although some studies have reported bimodal or trimodal distributions of adipocyte sizes [44, 50, 51], we did not observe such patterns in any of the conditions studied [37]. Across all groups, adipocyte diameters followed a normal distribution, with pre-BS obese patients displaying larger cells. Following BS and weight normalization, adipocyte size distribution was restored. The reduction in hypertrophy likely contributed to improved metabolic function, as larger adipocytes are associated with T2D, metabolic dysfunction, and a diminished capacity of AT to store lipids or release free fatty acids [16].

Low-grade inflammation in adipose tissue (AT) is a key contributor to the development of obesity-associated insulin resistance and cardiovascular disease [52, 53]. In line with our proteomic findings, which showed down-regulation of immune-related proteins after bariatric surgery (BS), S100A8 mRNA expression was elevated in obesity and decreased following BS in aSAT. These observations are consistent with previous studies. In humans, circulating S100A8/A9 levels have been linked to both insulin resistance [54] and obesity [54, 55], with higher levels associated with persistent diabetes after BS.

Specifically, reductions in circulating S100A8/A9 were observed in diabetic patients prior to, but not after, BS, and in non-diabetic individuals, but not consistently in diabetic subjects both before and after BS [56]. Additionally, studies in mice and humans indicate that S100A8 plays a role in recruiting macrophages into AT [36, 57]. Beyond immune-related proteins, weight loss also led to a decrease in oxidative stress–related proteins, such as peroxiredoxin-2 (PRDX2; $p = 1.46 \times 10^{-10}$), which has been implicated in linking inflammation and oxidative stress and is associated with TNF α production [58].

Although AT inflammation is well-known to promote insulin resistance, its exact cause remains uncertain. AT hypoxia has been proposed as one potential mechanism [59], but Woo et al. recently suggested that mitochondrial dysfunction in adipocytes may be a primary driver of inflammation [60]. Their work demonstrated that mitochondrial integrity in white adipocytes is crucial for adiponectin production and that thiazolidinedione treatment enhances insulin sensitivity and adiponectin levels by increasing mitochondrial content [60]. In morbidly obese populations, an inverse relationship between inflammation and mitochondrial function has been observed: AT and SAT from insulin-resistant and T2D individuals show reduced mitochondrial density [61– 63], limiting mitochondria-derived energy for lipogenesis. Dysfunctional mitochondria in human white AT may also promote the release of lipid metabolites and lactate, which are linked to peripheral insulin resistance [31]. In our study, multiple proteins involved in the citric acid cycle, respiratory electron transport, and ATP generation via chemiosmotic coupling were upregulated following BS. We also showed that obesity reduced mitochondrial coverage and density, which were restored after BS, highlighting the connection between mitochondrial dysfunction in aSAT and obesity. Mitochondrial coverage and density were inversely correlated with inflammation and positively associated with glucose uptake, lipogenesis, and insulin sensitivity. Additionally, tumor protein D54 (TPD54), which increased markedly after weight loss, has recently been localized to mitochondria; knockdown of TPD54 has been suggested to impair pyruvate dehydrogenase activity, reducing mitochondrial oxidative phosphorylation [64].

Our study has several strengths but also some limitations. The sample size of post-BS patients was small, limiting our ability to assess differences by sex, type of surgery, or comorbidities such as T2D. Furthermore, only a specific adipose biopsy area was analyzed, so regional variations in fat depth could not be accounted for. Nevertheless, the proteome was highly consistent across patients, and the analysis of genes, proteins, and mitochondrial morphometrics corroborated the proteomic data, reinforcing the robustness of our findings.

Future research should monitor these parameters longitudinally in larger cohorts to determine which changes are directly attributable to weight loss and which improvements occur independently of substantial weight reduction.

Conclusions

To our knowledge, this study represents the first "labelfree" quantitative proteomics analysis employing the SWATH-MS approach to identify proteins in aSAT whose expression is altered following weight loss induced by bariatric surgery. The pathways and protein classes most affected were associated with metabolism, immune regulation, and mitochondrial function, among others. Furthermore, we identified specific molecular mechanisms, genes, and proteins that contribute to improved adipose tissue function, including reduced inflammation, enhanced glucose uptake, increased insulin sensitivity, elevated de novo lipogenesis, improved mitochondrial performance, and smaller adipocyte size. Collectively, these findings indicate that bariatric surgery reshapes aSAT functionality, which likely underlies the metabolic benefits observed both locally in adipose tissue and systemically.

Supplementary Materials

The supplementary data are available online at https://www.mdpi.com/2077-0383/9/1/213/s1:

- Table S1: Enriched GO terms, protein classes, and biological pathways identified among proteins differentially expressed with body weight changes.
- Table S2: List of proteins quantified by SWATH-MS in aSAT from the same patients before and after bariatric surgery—induced weight loss, sorted by p-value. BS = bariatric surgery.
- \bullet Table S3: GO categories significantly enriched (adjusted p < 0.05) in proteins regulated by weight loss, based on FunRich analysis.
- \bullet Table S4: Reactome pathway enrichment for proteins significantly altered by weight loss following bariatric surgery, quantified using SWATH-MS, with a p-value cutoff of <10-5.
- Table S5: Anthropometric and biochemical parameters of patients analyzed by Western blot; values are presented as mean \pm SEM. Statistical differences are indicated by different letters (p < 0.05).
- Table S6: Anthropometric and biochemical data for patients analyzed by quantitative real-time PCR; values are expressed as mean \pm SEM, with statistically significant differences denoted by different letters (p < 0.05).

Acknowledgments: None.

Conflict of interest: None.

Financial support: None.

Ethics statement: None.

References

- Jastreboff AM, Kotz CM, Kahan S, Kelly AS, Heymsfield SB. Obesity as a disease: The obesity society 2018 position statement. Obesity (Silver Spring). 2019;27:7–9.
- 2. Bray GA, Heisel WE, Afshin A, Jensen MD, Dietz WH, Long M, et al. The science of obesity management: An endocrine society scientific statement. Endocr Rev. 2018;39:79–132.
- 3. Heymsfield SB, Wadden TA. Mechanisms, pathophysiology, and management of obesity. N Engl J Med. 2017;376:254–66.
- Ogrodnik M, Zhu Y, Langhi LGP, Tchkonia T, Kruger P, Fielder E, et al. Obesity-induced cellular senescence drives anxiety and impairs neurogenesis. Cell Metab. 2019;29:1061–77.
- Flegal KM, Graubard BI, Williamson DF, Gail MH. Cause-specific excess deaths associated with underweight, overweight, and obesity. JAMA. 2007;298:2028–37.
- Apovian CM. Obesity: Definition, comorbidities, causes, and burden. Am J Manag Care. 2016;22:S176–85.
- 7. Dye L, Boyle NB, Champ C, Lawton C. The relationship between obesity and cognitive health and decline. Proc Nutr Soc. 2017;76:443–54.
- 8. Gray SL, Vidal-Puig AJ. Adipose tissue expandability in the maintenance of metabolic homeostasis. Nutr Rev. 2007;65:S7–12.
- 9. Di Taranto G, Cicione C, Visconti G, Isgro MA, Barba M, Di Stasio E, et al. Qualitative and quantitative differences of adipose-derived stromal cells from superficial and deep subcutaneous lipoaspirates: A matter of fat. Cytotherapy. 2015;17:1076–89.
- 10. Tandon P, Wafer R, Minchin JEN. Adipose morphology and metabolic disease. J Exp Biol. 2018;221:jeb–164970.
- 11. Stefan N, Kantartzis K, Machann J, Schick F, Thamer C, Rittig K, et al. Identification and characterization of metabolically benign obesity in humans. Arch Intern Med. 2008;168:1609–16.
- Klein S, Fontana L, Young VL, Coggan AR, Kilo C, Patterson BW, et al. Absence of an effect of liposuction on insulin action and risk factors for coronary heart disease. N Engl J Med. 2004;350:2549–57.

- 13. Frayn KN. Adipose tissue as a buffer for daily lipid flux. Diabetologia. 2002;45:1201–10.
- Borges MC, Oliveira IO, Freitas DF, Horta BL, Ong KK, Gigante DP, et al. Obesity-induced hypoadiponectinaemia: The opposite influences of central and peripheral fat compartments. Int J Epidemiol. 2017;46:2044–55.
- 15. Vegiopoulos A, Rohm M, Herzig S. Adipose tissue: Between the extremes. EMBO J. 2017;36:1999–2017.
- Frikke-Schmidt H, O'Rourke RW, Lumeng CN, Sandoval DA, Seeley RJ. Does bariatric surgery improve adipose tissue function? Obes Rev. 2016;17:795–809.
- 17. Purnell JQ, Selzer F, Wahed AS, Pender J, Pories W, Pomp A, et al. Type 2 diabetes remission rates after laparoscopic gastric bypass and gastric banding: Results of the longitudinal assessment of bariatric surgery study. Diabetes Care. 2016;39:1101–7.
- 18. Kadera BE, Lum K, Grant J, Pryor AD, Portenier DD, DeMaria EJ. Remission of type 2 diabetes after Roux-en-Y gastric bypass is associated with greater weight loss. Surg Obes Relat Dis. 2009;5:305–9.
- Hamza N, Abbas MH, Darwish A, Shafeek Z, New J, Ammori BJ. Predictors of remission of type 2 diabetes mellitus after laparoscopic gastric banding and bypass. Surg Obes Relat Dis. 2011;7:691–696.
- Toro-Ramos T, Goodpaster BH, Janumala I, Lin S, Strain GW, Thornton JC, et al. Continued loss in visceral and intermuscular adipose tissue in weightstable women following bariatric surgery. Obesity (Silver Spring). 2015;23:62–9.
- Perez-Hernandez D, Gutierrez-Vazquez C, Jorge I, Lopez-Martin S, Ursa A, Sanchez-Madrid F, et al. The intracellular interactome of tetraspanin-enriched microdomains reveals their function as sorting machineries toward exosomes. J Biol Chem. 2013;288:11649–61.
- 22. Bonzon-Kulichenko E, Perez-Hernandez D, Nunez E, Martinez-Acedo P, Navarro P, Trevisan-Herraz M, et al. A robust method for quantitative high-throughput analysis of proteomes by 18O labeling. Mol Cell Proteomics. 2011;10:M110–003335.
- Shevchenko A, Wilm M, Vorm O, Jensen ON, Podtelejnikov AV, Neubauer G, et al. A strategy for identifying gel-separated proteins in sequence databases by MS alone. Biochem Soc Trans. 1996;24:893–6.
- 24. Shilov IV, Seymour SL, Patel AA, Loboda A, Tang WH, Keating SP, et al. The Paragon algorithm, a next generation search engine that uses sequence temperature values and feature probabilities to identify peptides from tandem mass spectra. Mol Cell Proteomics. 2007;6:1638–55.

- 25. Mi H, Muruganujan A, Huang X, Ebert D, Mills C, Guo X, et al. Protocol update for large-scale genome and gene function analysis with the PANTHER classification system (v.14.0). Nat Protoc. 2019;14:703–21.
- 26. Pathan M, Keerthikumar S, Ang CS, Gangoda L, Quek CY, Williamson NA, et al. FunRich: An open access standalone functional enrichment and interaction network analysis tool. Proteomics. 2015;15:2597–601.
- Szklarczyk D, Morris JH, Cook H, Kuhn M, Wyder S, Simonovic M, et al. The STRING database in 2017: Quality-controlled protein-protein association networks, made broadly accessible. Nucleic Acids Res. 2017;45:D362–8.
- 28. Schneider CA, Rasband WS, Eliceiri KW. NIH Image to ImageJ: 25 years of image analysis. Nat Methods. 2012;9:671–5.
- Sangiao-Alvarellos S, Helmling S, Vazquez MJ, Klussmann S, Cordido F. Ghrelin neutralization during fasting-refeeding cycle impairs the recuperation of body weight and alters hepatic energy metabolism. Mol Cell Endocrinol. 2011;335:177–88.
- 30. Fischer AH, Jacobson KA, Rose J, Zeller R. Hematoxylin and eosin staining of tissue and cell sections. CSH Protoc. 2008;2008:pdb-prot4986.
- 31. Bodis K, Roden M. Energy metabolism of white adipose tissue and insulin resistance in humans. Eur J Clin Invest. 2018;48:e13017.
- 32. Kahn SE, Hull RL, Utzschneider KM. Mechanisms linking obesity to insulin resistance and type 2 diabetes. Nature. 2006;444:840–6.
- 33. Bridges D, Saltiel AR. Phosphoinositides: Key modulators of energy metabolism. Biochim Biophys Acta. 2015;1851:857–66.
- 34. Averill MM, Kerkhoff C, Bornfeldt KE. S100A8 and S100A9 in cardiovascular biology and disease. Arterioscler Thromb Vasc Biol. 2012;32:223–9.
- 35. Unamuno X, Gomez-Ambrosi J, Rodriguez A, Becerril S, Fruhbeck G, et al. Adipokine dysregulation and adipose tissue inflammation in human obesity. Eur J Clin Invest. 2018;48:e12997.
- 36. Sekimoto R, Fukuda S, Maeda N, Tsushima Y, Matsuda K, Mori T, et al. Visualized macrophage dynamics and significance of S100A8 in obese fat. Proc Natl Acad Sci USA. 2015;112:E2058–66.
- 37. Hoffstedt J, Andersson DP, Eriksson Hogling D, Theorell J, Naslund E, et al. Long-term protective changes in adipose tissue after gastric bypass. Diabetes Care. 2017;40:77–84.
- 38. Hammarstedt A, Gogg S, Hedjazifar S, Nerstedt A, Smith U. Impaired adipogenesis and dysfunctional

- adipose tissue in human hypertrophic obesity. Physiol Rev. 2018;98:1911–41.
- Gancheva S, Jelenik T, Alvarez-Hernandez E, Roden M. Interorgan metabolic crosstalk in human insulin resistance. Physiol Rev. 2018;98:1371–415.
- Smith U, Kahn BB. Adipose tissue regulates insulin sensitivity: Role of adipogenesis, de novo lipogenesis and novel lipids. J Intern Med. 2016;280:465–475.
- 41. Winnier DA, Fourcaudot M, Norton L, Abdul-Ghani MA, Hu SL, Farook VS, et al. Transcriptomic identification of ADH1B as a novel candidate gene for obesity and insulin resistance in human adipose tissue in Mexican Americans from the Veterans Administration Genetic Epidemiology Study (VAGES). PLoS ONE. 2015;10:e0119941.
- 42. Vogel MAA, Wang P, Bouwman FG, Hoebers N, Blaak EE, et al. A comparison between the abdominal and femoral adipose tissue proteome of overweight and obese women. Sci Rep. 2019;9:4202.
- 43. Turcot V, Lu Y, Highland HM, Schurmann C, Justice AE, Fine RS, et al. Protein-altering variants associated with body mass index implicate pathways that control energy intake and expenditure in obesity. Nat Genet. 2018;50:26–41.
- 44. Yang J, Eliasson B, Smith U, Cushman SW, Sherman AS. The size of large adipose cells is a predictor of insulin resistance in first-degree relatives of type 2 diabetic patients. Obesity (Silver Spring). 2012;20:932–938.
- 45. McLaughlin T, Sherman A, Tsao P, Gonzalez O, Yee G, Lamendola C, et al. Enhanced proportion of small adipose cells in insulin-resistant vs insulin-sensitive obese individuals implicates impaired adipogenesis. Diabetologia. 2007;50:1707–15.
- McLaughlin T, Deng A, Yee G, Lamendola C, Reaven G, et al. Inflammation in subcutaneous adipose tissue: Relationship to adipose cell size. Diabetologia. 2010;53:369–377.
- 47. Danforth E Jr. Failure of adipocyte differentiation causes type II diabetes mellitus? Nat Genet. 2000;26:13.
- 48. Heilbronn L, Smith SR, Ravussin E. Failure of fat cell proliferation, mitochondrial function and fat oxidation results in ectopic fat storage, insulin resistance and type II diabetes mellitus. Int J Obes Relat Metab Disord. 2004;28 Suppl 4:S12–21.
- 49. Johannsen DL, Tchoukalova Y, Tam CS, Covington JD, Xie W, et al. Effect of 8 weeks of overfeeding on ectopic fat deposition and insulin sensitivity: Testing the "adipose tissue expandability" hypothesis. Diabetes Care. 2014;37:2789–2797.
- 50. Fang L, Guo F, Zhou L, Stahl R, Grams J. The cell size and distribution of adipocytes from

- subcutaneous and visceral fat is associated with type 2 diabetes mellitus in humans. Adipocyte. 2015;4:273–9.
- 51. McLaughlin T, Lamendola C, Coghlan N, Liu TC, Lerner K, et al. Subcutaneous adipose cell size and distribution: Relationship to insulin resistance and body fat. Obesity (Silver Spring). 2014;22:673–80.
- 52. Lackey DE, Olefsky JM. Regulation of metabolism by the innate immune system. Nat Rev Endocrinol. 2016;12:15–28.
- 53. Kohlgruber A, Lynch L. Adipose tissue inflammation in the pathogenesis of type 2 diabetes. Curr Diabetes Rep. 2015;15:92.
- 54. Ortega FJ, Sabater M, Moreno-Navarrete JM, Pueyo N, Botas P, et al. Serum and urinary concentrations of calprotectin as markers of insulin resistance and type 2 diabetes. Eur J Endocrinol. 2012;167:569–78.
- 55. Mortensen OH, Nielsen AR, Erikstrup C, Plomgaard P, Fischer CP, et al. Calprotectin—A novel marker of obesity. PLoS ONE. 2009;4:e7419.
- 56. Lylloff L, Bathum L, Madsbad S, Grundtvig JLG, Nordgaard-Lassen I, et al. S100A8/A9 (Calprotectin), interleukin-6, and C-reactive protein in obesity and diabetes before and after Roux-en-Y gastric bypass surgery. Obes Facts. 2017;10:386–95.
- 57. Nagareddy PR, Kraakman M, Masters SL, Stirzaker RA, Gorman DJ, et al. Adipose tissue macrophages promote myelopoiesis and monocytosis in obesity. Cell Metab. 2014;19:821–35.
- 58. Salzano S, Checconi P, Hanschmann EM, Lillig CH, Bowler LD, et al. Linkage of inflammation and oxidative stress via release of glutathionylated peroxiredoxin-2, which acts as a danger signal. Proc Natl Acad Sci USA. 2014;111:12157–62.
- 59. Rasouli N. Adipose tissue hypoxia and insulin resistance. J Investig Med. 2016;64:830–2.
- 60. Woo CY, Jang JE, Lee SE, Koh EH, Lee KU. Mitochondrial dysfunction in adipocytes as a primary cause of adipose tissue inflammation. Diabetes Metab J. 2019;43:247–56.
- 61. Qatanani M, Tan Y, Dobrin R, Greenawalt DM, Hu G, et al. Inverse regulation of inflammation and mitochondrial function in adipose tissue defines extreme insulin sensitivity in morbidly obese patients. Diabetes. 2013;62:855–63.
- 62. Xie X, Sinha S, Yi Z, Langlais PR, Madan M, Bowen BP, et al. Role of adipocyte mitochondria in inflammation, lipemia and insulin sensitivity in humans: Effects of pioglitazone treatment. Int J Obes (Lond). 2017;42:213–20.
- 63. Bogacka I, Xie H, Bray GA, Smith SR. Pioglitazone induces mitochondrial biogenesis in human subcutaneous adipose tissue in vivo. Diabetes. 2005;54:1392–9.

64. Zhuang Y, Ly RC, Frazier CV, Yu J, Qin S, Fan XY, et al. The novel function of tumor protein D54 in regulating pyruvate dehydrogenase and metformin cytotoxicity in breast cancer. Cancer Metab. 2019;7:1.